The Nonstationary Flood Hydrology of an Urbanizing Arid Watershed

GUO YU,[a] JULIANNE J. MILLER,[a] BENJAMIN J. HATCHETT,[a] MARKUS BERLI,[a] DANIEL B. WRIGHT,[b] CRAIG MCDOUGALL,[c] AND ZHIHUA ZHU[d]

[a] *Division of Hydrologic Sciences, Desert Research Institute, Las Vegas, Nevada*
[b] *Department of Civil and Environmental Engineering, University of Wisconsin–Madison, Madison, Wisconsin*
[c] *Clark County Regional Flood Control District, Las Vegas, Nevada*
[d] *Guangdong Provincial Key Laboratory of Water Quality Improvement and Ecological Restoration for Watersheds, School of Ecology, Environment and Resources, Guangdong University of Technology, Guangzhou, China*

(Manuscript received 6 July 2022, in final form 17 September 2022)

ABSTRACT: The Las Vegas metropolitan area in Nevada has experienced extensive urban growth since 1950 coincident with regional and local climate change. This study explores the nonstationary flood history of the Las Vegas Wash (LVW) watershed by deconstructing it into its constituent physical drivers. Observations and reanalysis products are used to examine the hydroclimatology, hydrometeorology, and hydrology of flash flooding in the watershed. Annual peak flows have increased nonlinearly over the past seven decades, with an abrupt changepoint detected in the mid-1990s, which is attributed to the implementation of flood conveyance systems rather than changes in land use. The LVW watershed exhibits two pronounced flood seasons, associated with distinct synoptic atmospheric circulations: winter floods linked to inland-penetrating atmospheric rivers and summer floods linked to the North American monsoon. El Niño–Southern Oscillation also plays a role in modulating extreme rainfall and the resultant floods because annual maximum daily rainfall totals positively correlate with El Niño, with Spearman's correlation coefficient of 0.36 (p value < 0.05). Winter maximum daily rainfall totals have increased since 1950, whereas summer daily rainfall maxima have decreased. The trends in hydrometeorological drivers interact with urbanization to shift flood seasonality toward more frequent winter floods in the LVW watershed. A process-based understanding of the flood hydrology of the watershed also provides insights into flood frequency analysis and flood forecasting.

KEYWORDS: Flood events; Climate change; Climatology; Atmospheric river

1. Introduction

Since the mid-twentieth century, the Las Vegas metropolitan area in southern Nevada has undergone some of the fastest urbanization of anywhere in the United States, with a population increase from less than 35 000 in 1950 to 2.6 million in 2020 (U.S. Census Bureau 2020). Despite its arid climate, Las Vegas is subject to extreme rainfall and flash flooding. Indeed, five out of the twelve most extreme flash floods in terms of streamflow per unit watershed area across the United States occurred in the arid Southwest, including the catastrophic flood in Eldorado Canyon in 1974, approximately 80 km south of Las Vegas (Glancy and Harmsen 1975; Costa 1987). Additional catastrophic flash floods (e.g., in July 1975, July 1999, and August 2012) in Las Vegas caused fatalities and substantial damages to property (Randerson 1976; Li et al. 2003).

Urbanization in arid valleys of the southwestern United States has pronounced implications for and vulnerabilities to flood-producing runoff processes. Arid cities such as Las Vegas, Nevada, and Phoenix and Tucson, Arizona, typically urbanize from the valley floors outward onto the surrounding alluvial fans emanating from the mountains. Such growth progressively increases their vulnerability to orographically enhanced heavy rainfall and results in risks to life and property from flash flooding, debris flows, and landslides (e.g., Coe 2016; Ahmadalipour and Moradkhani 2019; Smith et al. 2019). Land-use changes increase imperviousness, which reduces infiltration capacities and surface roughness, leading to higher overland flow volumes and velocities (e.g., Sauer et al. 1983; Smith et al. 2005a,b; Beighley and Moglen 2003; Hodgkins et al. 2019; Wright et al. 2012; Yang et al. 2013). The elaboration of drainage networks via open channel conveyance structures and culverts decreases the hydrologic response time of urban basins (e.g., Leopold and Maddock 1953; Leopold 1968; Smith et al. 2002; Kennedy et al. 2013). Channel lining prohibits the transmission losses of ephemeral arid watercourses, which reduces in-reach infiltration and enhances flood peaks (e.g., McCuen 2002; Miller et al. 2012).

Urbanizing watersheds are not exempt from the impacts of global warming. Human-induced climate change has resulted in a 1.5°C increase in average temperature across the Southwest since the 1960s (Karl et al. 2009). This warming effect has driven a dramatic decline in snowpack and annual streamflows in western U.S. mountains (Barnett et al. 2008; Pierce et al. 2008; Siirila-Woodburn et al. 2021). Despite a consistent signal of decreasing water availability, the warming effects on heavy rainfall and floods in the Southwest are complex and poorly understood. For example, Mallakpour and Villarini (2017),

Denotes content that is immediately available upon publication as open access.

Supplemental information related to this paper is available at the Journals Online website: https://doi.org/10.1175/JHM-D-22-0117.s1.

Corresponding author: Guo Yu, guo.yu@dri.edu

DOI: 10.1175/JHM-D-22-0117.1

detected incidences of both increasing and decreasing trends in heavy daily-scale rainfall across the Southwest. Furthermore, the impacts of climate change-induced warmings on short-duration (e.g., 1–3 h) rainfall extremes are more complex because they are determined by the combined effects of large-scale atmospheric circulation, atmospheric stability, and local-scale dynamics of convective clouds (Fowler et al. 2021). Daily and subdaily rainfall intensities over the arid Southwestern United States, especially in the lower Colorado River basins, are projected to decline by the end of the twenty-first century by a variety of climate model simulations (Prein et al. 2017; Singer and Michaelides 2017; Hernandez and Chen 2022). The projected weakening North American monsoon (NAM) under warming climate will exacerbate such a decline of rainfall over the Southwestern United States (Pascale et al. 2017).

Numerous studies on the hydrological impacts of urbanization and climate change mainly focus on trend analysis (e.g., Choi et al. 2003; Burns et al. 2005; Jiang et al. 2007; Kilsby et al. 2007; Oudin et al. 2018). Such studies typically attribute trends in peak flows to trends in other explanatory variables, such as precipitation and imperviousness (e.g., Beighley and Moglen 2002; Petrow and Merz 2009; Korhonen and Kuusisto 2010). Fewer studies have assessed the nonstationarities in flood observations by jointly examining urbanization and climate change. In one example, Yang et al. (2013) found that urbanization, including its direct impact on heavy rainfall over the Milwaukee, Wisconsin, metropolitan area has caused increases in summer thunderstorms and the resultant flood peaks. Similarly, Merz and Blöschl (2008) investigated the climatic and nonclimatic processes to diagnose nonstationary flood characteristics and demonstrated that understanding such processes can improve the credibility of the estimated flood frequencies.

Floods at the watershed outlet or at a gauged location are the products of interactions between physical processes occurring in the atmosphere and on the land surface. Therefore, nonstationarity in streamflow observations, including secular trends and variability, must be ascribable to the changes in their underlying drivers. The objective of this study is to provide insights into the nonstationarity in historical peak flows for the Las Vegas Wash (LVW) watershed by examining its hydroclimatology, hydrometeorology, and hydrology. The aim of such a process-based approach is to investigate changes in the underlying processes and how they interact to shape the outcome (e.g., Culley et al. 2016; Yu et al. 2019; Wright et al. 2020; Yu et al. 2021).

Herein, we use a variety of observational data and model reanalysis products to obtain a process-based view of urban floods in the LVW watershed. This view extends from the synoptic-scale atmospheric circulations to the dynamics of heavy rainfall that becomes surface runoff. In addition, we examine climate-induced changes in flood agents and how they interact with urbanization to determine flood responses. Moreover, insights into these flood-generating processes facilitate improvement in flood management practices, such as flood frequency analysis, flood forecasting at subseasonal-to-seasonal time scales, and prioritizing infrastructure investments.

2. Study region

The LVW watershed is in the southern Basin and Range physiographic province, which is close to the geographical boundaries of Nevada, California, and Arizona (Fig. 1a). This watershed is characterized by a typical "Mojave Desert landscape"—with wind and water eroding and dispersing sediments from steep mountains to valley floors to form the alluvial fans in the basin on which the city has developed (Miller 2012; Fig. 1c). The Spring Mountains and Sheep Range, both with elevations higher than 2500 m above sea level (MSL), border the valley on the west and north sides, respectively. Several small mountains higher than 800 m MSL are located on the southern and eastern sides of the valley. According to the 2019 National Land Cover Database (NLCD), the land use is designated as mainly developed for the valley, whereas mountainous regions are designated as shrubland and forest (Fig. 1c).

The main stem of the LVW extends northwest to southeast through the Las Vegas Valley, terminating in Lake Mead, which is part of the Colorado River basin (Fig. 1a). The contributing drainage area for the LVW watershed is 4084 km^2, within which 26% (1080 km^2; red line in Fig. 1b) is the developed Las Vegas metropolitan area. Five subbasins—Gowan, Central, Flamingo, Duck Creek, and Pittman—drain the valley eastward to the LVW, accounting for 74% (796 km^2) of the urban area (Fig. 1b). The LVW watershed experienced substantial changes in land use because of urbanization over the past seven decades (Fig. 1c).

3. Data and methods

a. Data

1) Land-use and land-cover data

The remote sensing-based NLCD provides land use and impervious cover maps for the conterminous United States (CONUS) from 2001 to 2019 at 2–3-yr intervals (Fry et al. 2011; Homer et al. 2020). To assess long-term spatial and temporal changes in land use, U.S. Geological Survey modeled historical land-use (USGS-LU) data were applied (Sohl et al. 2016). The USGS-LU uses numerous historical data sources and a spatially explicit modeling framework to "backcast" land use and land cover for the CONUS at annual, 250-m resolution for the 1938–92 period. The trends and spatial pattern of the USGS-LU are comparable to results based on other independent historical data sources, such as housing density data by the U.S. Census Bureau (Sohl et al. 2016).

Here, we collected land-use data for the LVW watershed for the 1950–2019 period using both the USGS-LU and NLCD. Land use was categorized into five classes: developed, barren land, shrubland, forest, and open water/wetland (Fig. 1c). Imperviousness (%) is only available in the NLCD (thus, only the 2001–19 period). Therefore, we calculated the mean imperviousness for the developed areas (imperviousness is zero for other land uses) for the 2001–19 period, which is 58%. This value was then used to estimate the imperviousness for the LVW watershed for the 1950–92 period based on the percentage of developed area within the watershed.

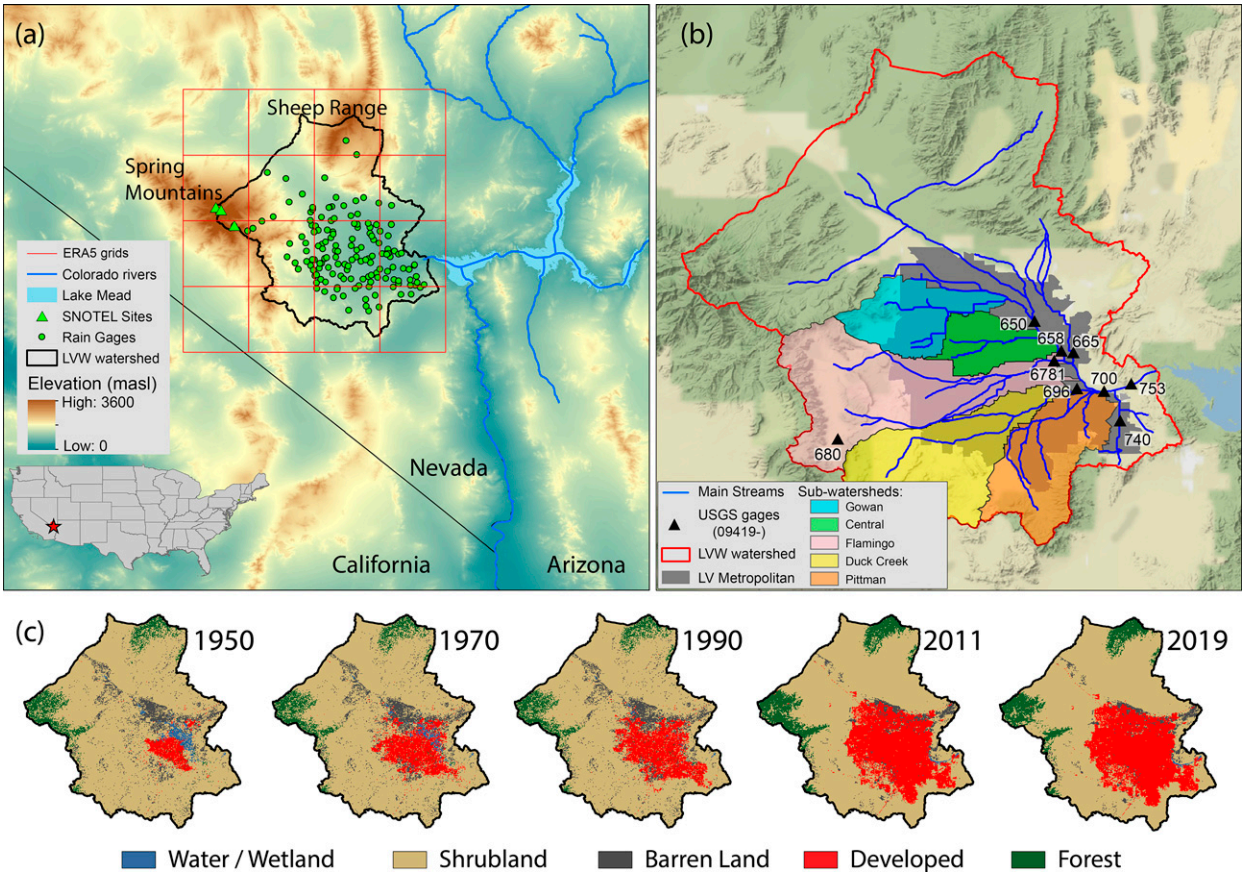

FIG. 1. (a) The location of the Las Vegas Wash (LVW) watershed and rain gauges are shown with the elevations. The inset map shows the conterminous United States, and the red star indicates the location of the watershed. (b) The locations of nine U.S. Geological Survey (USGS) streamflow stations along with the main streams of the LVW watershed, as well as the five main subbasins that drain 74% of the metropolitan area. The gray shaded area shown within the LVW watershed denotes the Las Vegas metropolitan area based on 2020 U.S. Census Bureau data. (c) Changes in land use for LVW watershed from 1950 to 2019 are shown. Land-use data from 1950, 1970, and 1990 are from USGS-LU, whereas NLCD data are used for 2011 and 2019.

2) VERTICALLY INTEGRATED WATER VAPOR TRANSPORT (IVT)

To understand the flood-generating mechanisms for the LVW watershed from a synoptic scale, we calculated the daily vertically integrated water vapor transport (IVT), which represents "the fuel for precipitation," using ERA5 reanalysis (Hersbach et al. 2020). ERA5 reanalysis is at 31-km spatial and hourly temporal resolution and is available from 1950 to the present. Daily IVT is selected over the daily integrated water vapor (IWV) because a previous study demonstrated that IVT was more strongly correlated with precipitation over the western United States than IWV, especially during the winter season (Rutz et al. 2014). The IVT is calculated as follows:

$$\mathrm{IVT} = \left\{\left[\frac{1}{g}\int_{p(\mathrm{sfc})}^{300\,\mathrm{hpa}} qu\,dp\right]^2 + \left[\frac{1}{g}\int_{p(\mathrm{sfc})}^{300\,\mathrm{hpa}} qv\,dp\right]^2\right\}^{1/2}, \quad (1)$$

where q is the specific humidity (kg kg^{-1}), u is the zonal layer-averaged wind (m s^{-1}), v is the meridional layer-averaged wind (m s^{-1}), and g is the gravitational constant (9.8 m s^{-2}). Variable p(sfc) is the pressure level (hpa) at the land surface, and dp is the pressure difference between two vertical levels. We calculated basin-averaged daily IVT for the LVW watershed for the 1951–2020 period.

3) METEOROLOGICAL DATA

To assess the long-term precipitation trends for the LVW watershed, we derived basin-averaged daily rainfall (all rainfall values shown are basin-averaged values unless further clarification is given) using the 1951–2020, 5-km and daily National Oceanic and Atmospheric Administration (NOAA) Climate Gridded dataset (NClimGrid; Vose et al. 2014). The NClimGrid is based on multiple sources of station data, including the Global Historical Climatology Network, Cooperative Observer Program, Automated Surface Observing System, National Interagency Fire Center Remote Automatic Weather Station, and the U.S. Department of Agriculture Snow Telemetry (SNOTEL) network.

The Clark County Regional Flood Control District (CCRFCD) maintains a dense network of 153 rain gauges

(one per 27 km^2) which were used to characterize the spatial and temporal structure of rainfall (Fig. 1a). In total, 58 (38%) gauges became operational in 1996 and the majority (>50%) were operational by 2000. These rain gauges report on irregular intervals ranging from 1 to 30 min. These observations were aggregated or linearly interpolated to 15-min resolution in this study.

Daily snow water equivalent (SWE) and mean temperature data for the 2008–20 period were collected from three SNOTEL sites in the Spring Mountains (Fig. 1a), with elevations ranging from 2400 to 2700 MSL. The mean values of daily SWE and temperature for three SNOTEL sites were used for trend analyses.

4) Streamflow data

Nine USGS streamflow gauges within the LVW watershed were used with records ranging from 22 to 53 years of annual peak flows (Fig. 1b). The gauge at the watershed outlet (USGS: 09419800; drainage area: 4084 km^2) does not provide continuous long-term annual peak flows. Therefore, two gauges (USGS: 09419700 and 09419753) that have similar drainage areas and are in the vicinity of the watershed outlet were combined to provide peak flows for the 1957–2020 period, which represents the records at the watershed outlet. Stream gauges at the LVW above Three Kids Wash (USGS: 09419753) and at Pabco Road (USGS: 09419700) are 5 and 9 km upstream from the watershed outlet, respectively. Their drainage areas account for 99% and 96% of the total watershed area, respectively.

5) River networks and detention basins

Natural river networks for the LVW watershed are based on USGS National Hydrography Dataset Plus Version 2 stream reaches (NHDPlus V2; Moore and Dewald 2016). The NHDPlus V2 provides vector-based stream networks and associated attributes, such as channel length and slopes. Data for flood conveyance systems, including constructed river networks and detention basins, are provided by the CCRFCD.

b. Methods

1) Trend analysis and changepoint detection

Trend analyses were applied to land use and several hydrometeorological variables for the 1950–2020 period. These variables include annual peak flows, annual maximum basin-averaged daily rainfall, annual maximum daily rainfall in summer and winter, and annual 95th percentiles of daily IVT in summer and winter. Winter (i.e., cold season) and summer (i.e., warm season) for the LVW watershed are defined hereafter as October–March and April–September, respectively. Trends were assessed using both the nonparametric Mann–Kendall test (M–K; Mann 1945; Kendall 1975) for monotonic trends and the Theil–Sen nonparametric linear regression (T–S; Sen 1968). The Pettitt test was applied to annual peak flows for changepoint detection (Pettitt 1979).

2) Width function calculations

The width function (Lee and Delleur 1976) for river networks is defined as the number of channel links at a specified distance from the outlet. It represents the spatial distribution of drainage pathways with respect to travel distance. Under the assumption of uniform rainfall and constant flow velocity, width function resembles the flood hydrograph (e.g., Gupta and Mesa 1988; Rodríguez-Iturbe and Rinaldo 2001; Veitzer and Gupta 2001; Perez et al. 2018). It has therefore been widely used to understand and model streamflow response, often in combination with the instantaneous unit hydrograph (e.g., Gupta et al. 1980; Kirshen and Bras 1983; Tarboton et al. 1989). The width function takes the following form:

$$W(x) = \text{Count}[x - \Delta x < D(\text{link}) < x], \tag{2}$$

where Count(x) is the count of stream links that conform to the condition in the parentheses. D(link) is the distance from the link to the watershed outlet, x is the distance to be evaluated, and Δx is the width interval, which is defined as 2 km in this study.

4. Results

a. Hydrological impacts of urbanization

Annual flood peaks for the outlet of LVW watershed show increases in both magnitude and variability during the 1957–2020 period (Fig. 2a). Nonparametric M–K and T–S tests show significant (p value < 0.05) increasing trends in annual flood peaks, and a nonparametric Pettitt test detects a changepoint to annual peak flows in 1996 (Fig. 2a and Table 1). To add confidence in the Pettitt test, a Monte Carlo bootstrap resampling procedure was performed where flood peaks were randomly sampled 1000 times and the test was applied to each sample. Only in 28 out of 1000 cases were changepoints in the random samples also identified (effective p value = 0.028), providing additional confidence in the robustness of the identified changepoint from the observed data.

During the second half of the period (1989–2020), 29 out of 32 (91%) annual flood peaks are higher than the median annual flood peaks (38 m^3 s^{-1}). The change in extreme flood events is also notable, with the largest nine flood peaks having occurred during the second half of the period and after the detected changepoint in 1996. In addition, flood peaks at all USGS stream gauges exhibit increasing trends except for one gauge located in a headwater catchment where urbanization has not occurred (Fig. S1 in the online supplemental material).

The relationship between annual flood peaks and their corresponding daily rainfall totals underscores the elevated flood peaks during the last three decades (Fig. 2b). The median rainfall totals and peak flows for the first half of the period are 16 mm and 15 m^3 s^{-1}, whereas the corresponding values for the second half of the period are 18 mm and 89 m^3 s^{-1}. Consequently, relatively similar amounts of daily rainfall produced smaller flood peaks in earlier years and larger peaks in recent years (Fig. 2b). However, there is no significant increase in the annual maximum daily rainfall and rainfall variability

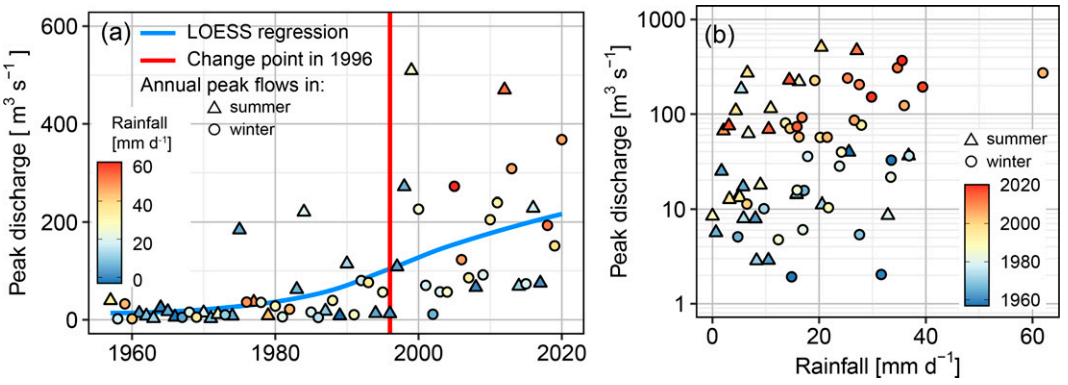

FIG. 2. (a) Annual peak flows for the LVW watershed over the 1957–2020 period and (b) their corresponding daily rainfall totals. Blue and red lines in (a) represent the locally weighted polynomial regression (LOESS; Cleveland 1979) and Pettitt test changepoint fitted to all annual peak flows, respectively. Peak flows in both subplots are distinguished by their season.

(i.e., standard deviation) over the past seven decades based on nonparametric M–K and T–S tests (Table 1). Therefore, changes in daily rainfall are not sufficient to explain the elevated flood peaks in recent years for the LVW watershed (Fig. 2a). However, the analyses confirm that summer storms typically generate higher peak flows than winter storms regardless of time period (Fig. 2b). This is mainly due to the spatial and temporal structure of summer rainfall and will be discussed in section 4c.

Land-use change has predominantly occurred along the valley margins, with urban development growing outward from the valley floor onto surrounding alluvial fan surfaces (Fig. 3). Within the LVW watershed, developed land has increased from 134 km^2 (3.3% of watershed area) to 998 km^2 (24.4%) over the past seven decades, replacing natural land-use types (Fig. 3c and Fig. S2). The developed land class and associated imperviousness in the Las Vegas Valley using a combination of USGS-LU and NLCD show a roughly linear increase from 1951 to 2020 (Fig. 3c and Table 1). This linear behavior contrasts with the nonlinear increase and step change in annual peak flows (Figs. 2a, 3c).

Flood control facilities, including drainage networks and detention basins, have been implemented by the CCRFCD since its establishment in 1985 (Figs. 4a–c). To convey surface runoff safely and efficiently to the LVW and eventually to Lake Mead, the CCRFCD has constructed and lined over 1000 km of storm drains and open channels in the valley with concrete (Figs. 4a–c). This has caused drainage density in the Las Vegas Valley to increase from 0.36 to 0.74 km^{-1}. The increased density of conveyance facilities shortens the distance between the surface and channel, and rapidly conveys in-channel flows downstream, leading to faster hydrologic response times and larger flood peaks. Of these channels, 74% (792 km) were built after 1996 (Fig. 4c), the year that was identified as the changepoint in annual flood peaks (Fig. 2a).

The width function for the river network after the implementation of flood conveyance system shows a striking change compared with the natural channel network (Fig. 4d). These constructed channels are concentrated in the lower portion of the LVW watershed (i.e., within the developed area), between 20 and 60 km away from its outlet. The enhanced width function indicates increased drainage density and more network "links" that can simultaneously contribute to the main stem, leading to higher flood peaks and shorter times to peak. The width function strongly points to the role of built conveyance in enhancing flood peaks in recent decades (Figs. 4d, 2a).

Besides conveyance facilities, 59 major detention basins were constructed within the LVW watershed between 1990 and 2020, with a total capacity exceeding 50 million m^3 (Figs. 4a–c; see Fig. S3 for a photo of the largest detention basin). The largest of these basins have been built along the margins of the valley, downstream of the apexes of large alluvial fans to capture flows

TABLE 1. Trend analyses for a variety of hydrological variables and imperviousness. Significant trends at the 5% level are shown in bold.

Variables	Period	M–K trend (p value)	T–S slope (p value)
Annual peak flows	1957–2020	↑ **(<0.001)**	**1.573 (<0.001)**
Annual max daily rainfall	1951–2020	↑ (0.435)	0.023 (0.219)
Daily rainfall variability	1951–2020	↑ (0.801)	−0.003 (0.551)
Imperviousness	1951–2020	↑ **(<0.001)**	**0.514 (<0.001)**
95th percentile of daily IVT in summer	1951–2020	↓ (0.052)	**−0.214 (<0.001)**
95th percentile of daily IVT in winter	1951–2020	↑ (0.598)	0.066 (0.508)
95th percentile of daily CAPE in summer	1951–2020	↑ (0.183)	2.022 (0.237)
Annual max daily rainfall in summer	1951–2020	↓ (0.093)	**−0.108 (<0.001)**
Annual max daily rainfall in winter	1951–2020	↑ **(0.035)**	**0.191 (<0.001)**

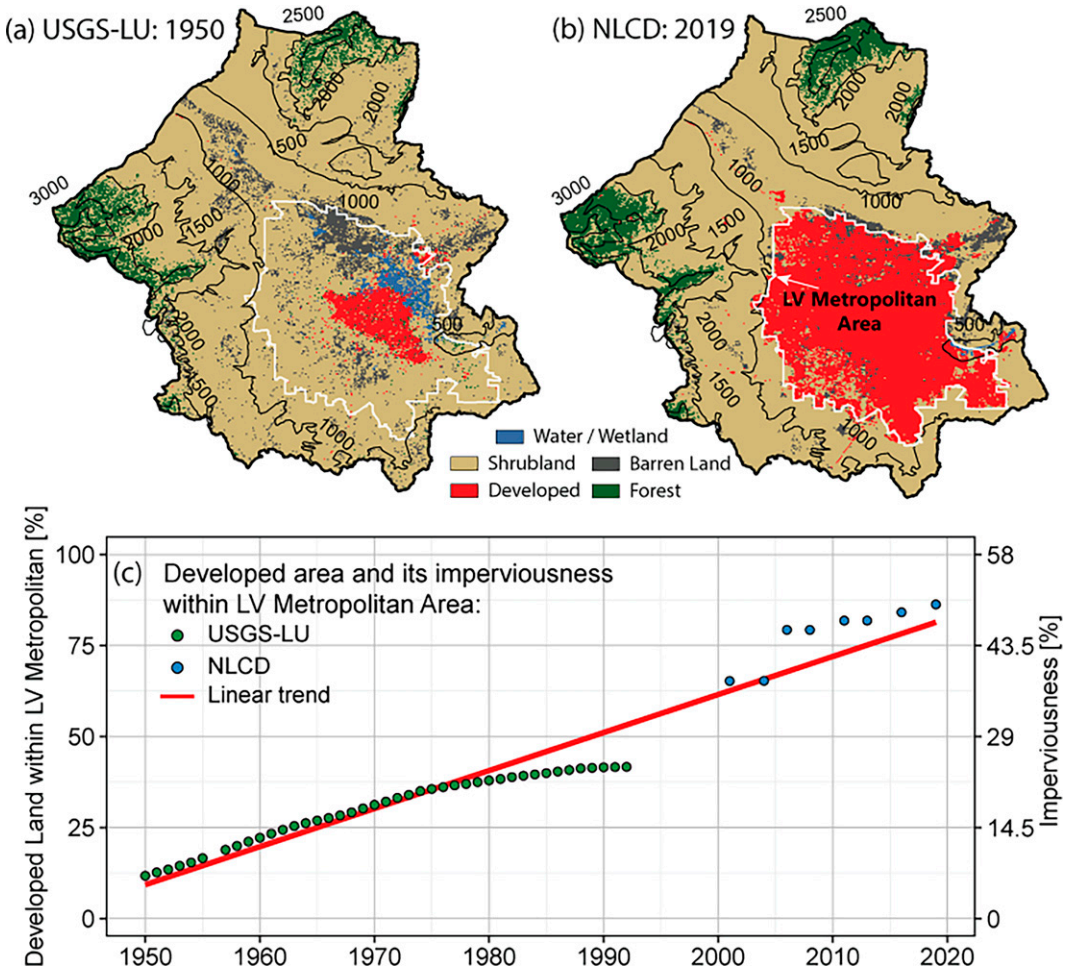

FIG. 3. The land use for LVW watershed in (a) 1950 and (b) 2019. (c) The variations in percentages of developed land within the Las Vegas metropolitan area and the corresponding imperviousness from 1950 to 2019. Contour lines in (a) and (b) represent elevation (m MSL). The red line in (c) denotes a linear regression fitted to percentages of developed land within the Las Vegas metropolitan area. See Fig. 1c for the land-use changes in every ~20 years.

emanating from the mountains. These detention basins mitigate for the loss of the "natural flood buffer zones" of these now-developed alluvial fans (Fig. S4). Prior to development, the large surface areas of the natural alluvial fans reduced the volume of flood flows that reached the valley center by minimizing flow velocities and increasing channel transmission losses. However, this natural attenuation was lost as urbanization encroached (Fig. S4). Now, the large detention basins provide this attenuation function by controlling releases of detained flood waters through the constructed system of conveyance channels that cross the valley. To further attenuate flood waves, additional detention basins were built along the conveyance channels, which tend to be smaller because of limited space within the more urbanized portions of the valley (Fig. 4).

The additional detention basins play an important role in attenuating flood peaks. Indicative of their successful implementation, none has been overtopped since construction. The largest volumes that have been detained in the large basins along the city margins have been less than 20% of the overall basin volume, whereas the smaller downstream basins have at times reached around 50% capacity (Fig. S5a). Based on rating curves for the detention basins, estimated maximum outflows for these basins are mostly less than 20 $m^3 s^{-1}$, which is quite low relative to their contributing drainage areas and peak flows at the watershed outlet (Fig. S5b). Because of limited space, there are no constructed basins for attenuating flood peaks within the southeastern part of the Las Vegas Valley. This points to a trade-off between land development and flood management.

Flood peaks for arid watersheds are weakly dependent on drainage area because of channel transmission loss, low connectivity, and the typically spatially limited nature of intense thunderstorms making them rare for substantial fractions of larger areas to contribute simultaneous flood flows (e.g., Thomas et al. 1997; Etheredge et al. 2004; Smith et al. 2019). The detention basins that attenuate flood flow from the large and mostly nonurban upstream areas further weaken the dependency of flood peaks on drainage area. The distributions

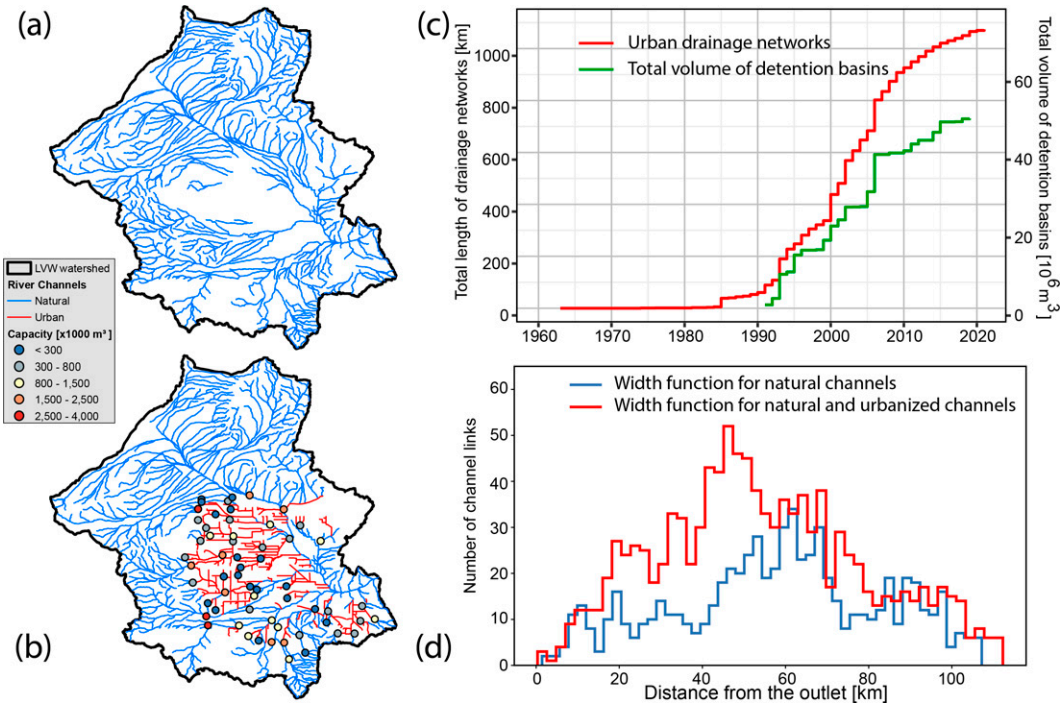

FIG. 4. Spatial distribution of river channels (a) without and (b) with flood conveyance systems. (c) Accumulated length of built drainage network and detention basin storage over time. (d) Width functions for river channels before and after the implementation of the built flood conveyance system. The average channel lengths for natural and constructed channels are 2.1 and 1.6 km, respectively.

of annual peak flows for the available period of record for each of the nine USGS gauges show that smaller, highly urban watersheds (e.g., 570 km^2 Flamingo Wash; median peak flows = 40 $m^3 s^{-1}$) can yield higher flood peaks than much larger, nonurban ones (e.g., 1990 km^2 LVW at North Las Vegas; median peak flows = 14 $m^3 s^{-1}$; Fig. S6 and Table S1).

b. *Rainfall and flood hydroclimatology*

The seasonalities of precipitation and floods for the LVW watershed exhibit two pronounced seasons: winter and summer (Fig. 5). A slight discrepancy between rainfall and flood seasonality in July–August is due to the heavy rainfall in summer (Fig. 5). Localized, short-duration convective summer storms with high rainfall intensities can result in substantial flash flooding despite their relatively small daily rainfall totals.

Rainfall and flood seasonality in the LVW watershed are attributable to two distinct large-scale atmospheric circulations. Winter floods are tied to upper-level low pressure systems situated over the Pacific Coast. Such systems steer the jet stream equatorward and drive storm tracks into Southern California, leading to a greater number of storms across the southwestern United States (Hirschboeck 1987a; Sheppard et al. 2002). Maddox et al. (1980) classified this synoptic weather feature as a "Western Type III" event. This weather pattern leads to increased likelihood of landfalling atmospheric rivers (ARs) along the Pacific Coast and some of these ARs, when favorable aligned with gaps in topography, can penetrate into interior regions of the western United States, causing regional extreme precipitation, flooding, and avalanches (e.g., Rutz et al. 2014, 2015; Swales et al. 2016; Hatchett et al. 2017; Albano et al. 2020). In addition, precipitation across the southwestern United States is teleconnected with El Niño–Southern Oscillation (ENSO) because El Niño typically enhances regional precipitation in winter (e.g., Redmond and Koch 1991; Cayan et al. 1999).

We found the Southern Oscillation index (SOI; NOAA 2022) significantly correlates with annual maximum daily rainfall, with a Spearman's correlation coefficient = 0.36 (p value < 0.05; Fig. 6). Other low-frequency modes of climate variability and their respective indices climatic indices, including Pacific decadal oscillation, North Atlantic Oscillation, and Pacific–North American pattern, have also been tested for their correlations with the annual maximum daily rainfall in the LVW watershed. We find these modes are less strongly correlated than SOI with the rainfall in the LVW watershed. Based on the Gershunov et al. (2017) AR catalog and the corresponding extent of AR-related precipitation (extended to 2020), we identified 25 annual rainfall maxima that resulted from inland-penetrating ARs (Fig. 6). These AR-related annual rainfall maxima show higher rainfall totals than the non-AR group, especially during El Niño years (Fig. 6). Furthermore, 19 (54%) of the 35 annual peak flows that occurred in winter were associated with ARs, highlighting the key role of ARs in generating winter-season floods in the LVW watershed.

The direction and landfall position of ARs also modulate the amount of water vapor transported into the watershed.

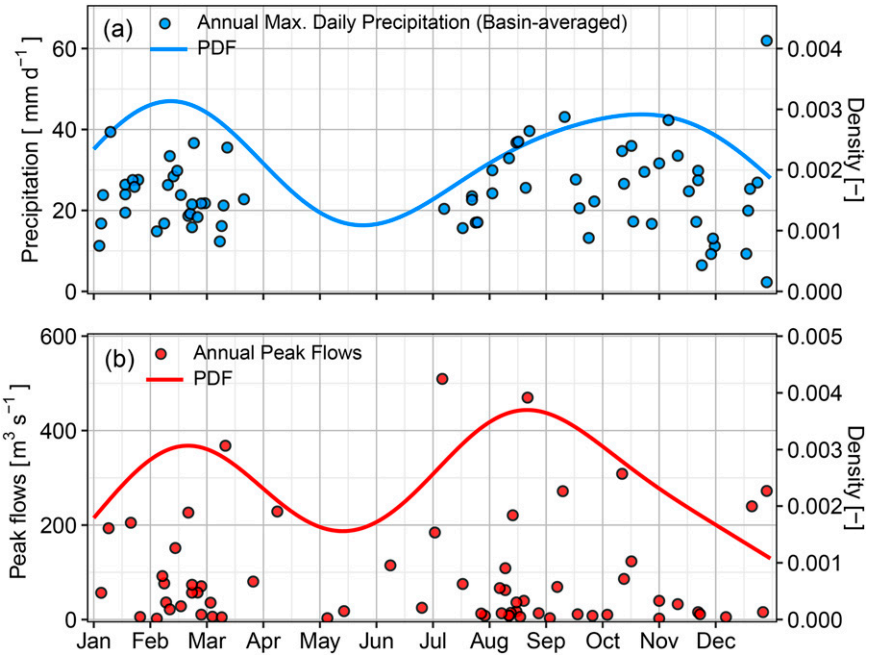

FIG. 5. The seasonality of annual maximum daily rainfall using (a) NClimGrid and (b) USGS peak flows for the 1957–2020 period.

When ARs make landfall over a broad region of the Pacific Southwest and move eastward to interior land, a substantial amount of water vapor will be blocked by the mountains of the Pacific Cordillera, including the Coast Ranges and Sierra Nevada, with less moisture penetrating into southern Nevada. For example, a strong AR [based on Ralph et al. (2019) AR scales] storm on 17 February 1980, only caused 24-mm daily rainfall over the LVW watershed (Figs. S7a,b). However, when ARs make landfall in Southern California and proceed northeast, the storms bypass the Sierra Nevada and bring more water vapor into southern Nevada. For example, on 29 December 2004, the record daily rainfall for the LVW watershed (62 mm) resulted from a moderate AR moving from Southern California (Figs. S7c,d).

Summer floods are typically linked to the NAM, which transports moisture northward from the eastern Pacific and the Gulfs of California and Mexico (e.g., Adams and Comrie 1997; Berg et al. 2000). Previous studies identified that the moisture over the Southwestern United States during the NAM season is transported from the Gulf of California and the eastern Pacific at a low level (i.e., "gulf surges"), but at the mid and high levels from the Gulf of Mexico (Higgins et al. 1998,

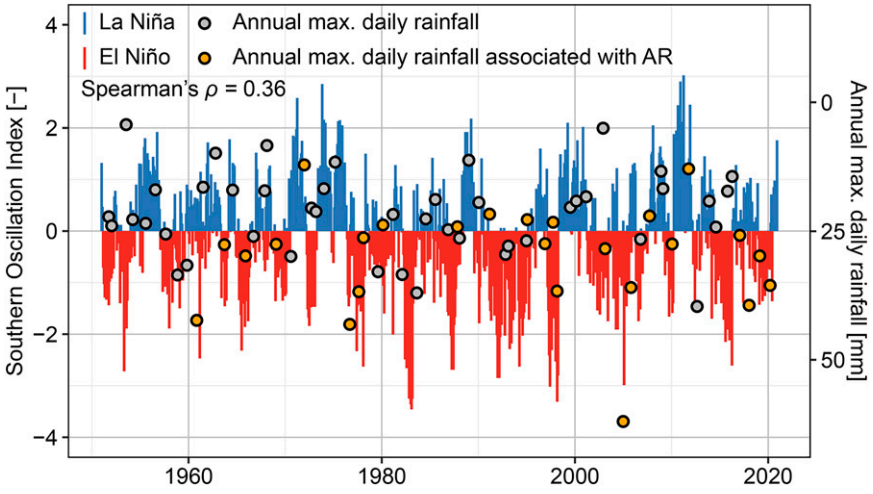

FIG. 6. The SOI and annual maximum daily rainfall teleconnection for the LVW watershed. Events associated with atmospheric rivers (ARs) are highlighted in orange.

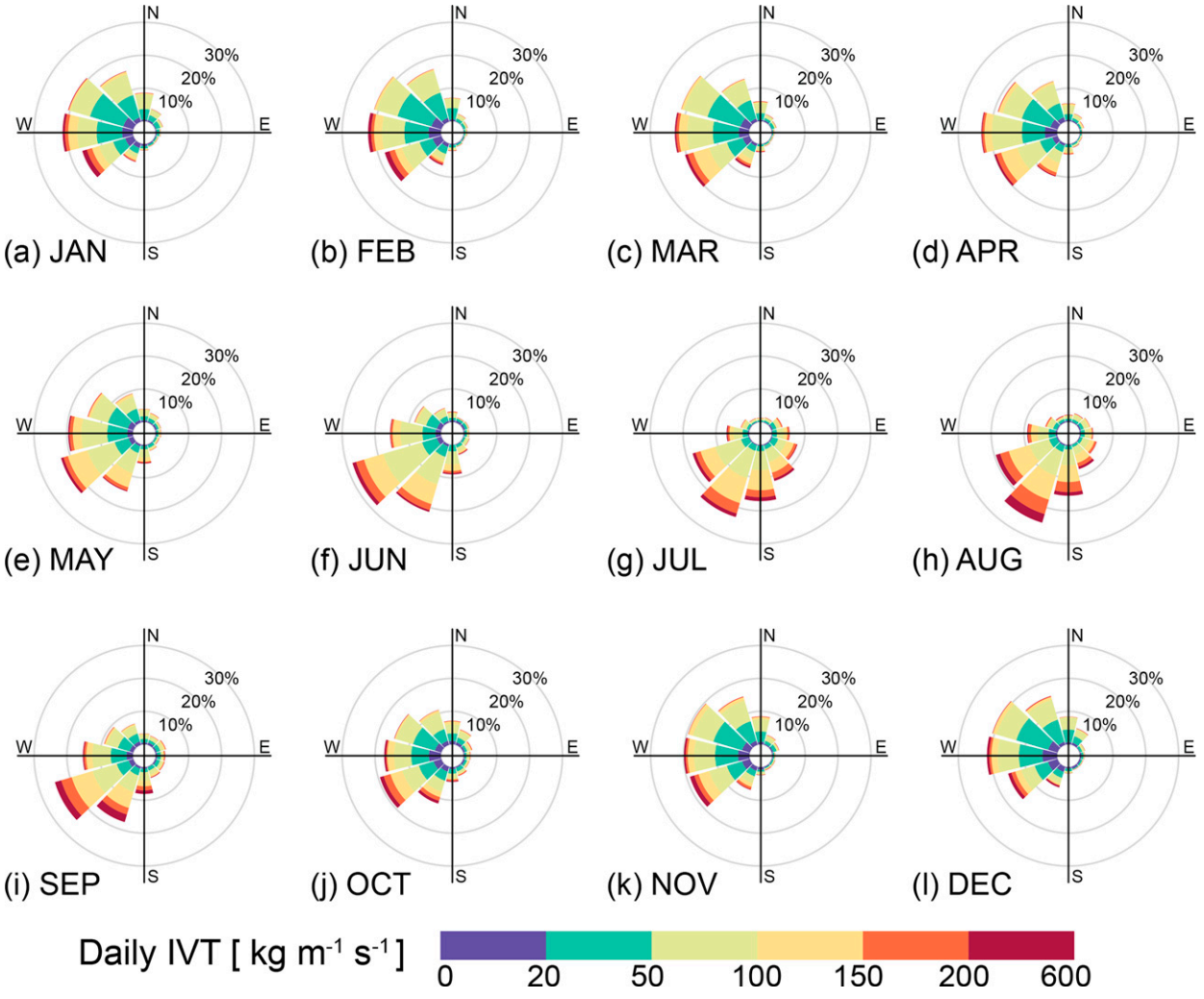

FIG. 7. Daily IVT for the LVW watershed during the 1951–2020 period. Each wind rose indicates the direction and distribution of the intensities of daily IVT.

1999; Wright et al. 2001). Occasionally, a large-scale NAM interacts with local-scale shortwave troughs to yield heavy rainfall (Western Type II and IV; Maddox et al. 1980). Based on cloud-to-ground lightning flash data from the U.S. National Lightning Detection Network for 1987–2020 (Koehler 2020), the annual mean number of flashes over the LVW watershed are 5638 in summer but only 488 in winter. This highlights the role of convective thunderstorms in producing intense rainfall in summer.

Although eastern Pacific tropical cyclones and their remnants rarely affect the weather in the LVW watershed (Smith 1986; Barth et al. 2018), they have caused four annual peak flows during the 1957–2020 period: September 1962 (8 $m^3 s^{-1}$), October 1972 (10 $m^3 s^{-1}$), August 1977 (36 $m^3 s^{-1}$), and September 1998 (272 $m^3 s^{-1}$).

The long-term climatology of IVT shows seasonal variations with respect to direction and intensity (Fig. 7). The main directions of IVT shift from westerly in January to southerly in July and back again, consistent with the directions of the moisture source associated with large-scale atmospheric circulations (Fig. 7). Specifically, the dominant moisture over the LVW watershed originates from the Pacific in winter and from the Gulf of California in summer. In addition, the daily IVT is stronger in summer than in winter, as shown by the percentage of IVT exceeding 200 kg $m^{-1} s^{-1}$, indicating the role of elevated moisture content of the atmosphere under warmer conditions (Fig. 7).

The 95th percentiles of daily IVT in summer show an insignificant (at the 5% level) decreasing trend using both M–K and T–S tests, whereas the 95th percentile of daily IVT in winter shows a significant (insignificant) increasing trend using the T–S (M–K) test (Table 1). The increase in extreme daily IVT in winter is in line with the thermodynamically driven (i.e., Clausius–Clapeyron) enhancement in the frequencies and magnitudes of ARs over the western United States (Polade et al. 2017; Gershunov et al. 2019; Rhoades et al. 2020; Baek and Lora 2021; Michaelis et al. 2022). Additionally, we found a significant decrease in the maximum convective available potential energy (CAPE) in summer for

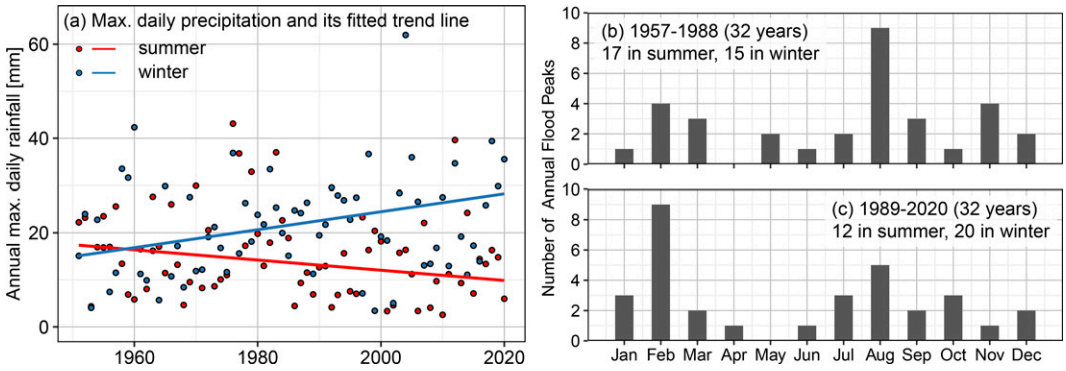

FIG. 8. (a) Annual maximum daily rainfall in summer and winter and the fitted T–S linear regressions. Both T–S linear regressions in (a) are significant at the 5% level. The number of annual flood peaks grouped by month for the (b) 1957–88 and (c) 1989–2020 periods.

the 1995–2020 period (not shown) using the sounding data at Desert Rock station (Augustine et al. 2000), indicating a decrease in atmospheric instability over the past three decades. The 95th percentiles of ERA5-based daily CAPE in summer show a consistent decrease for the overlapping period (1995–2020) with the sounding data whereas we find an insignificant increase for the 1951–2020 period (Table 1).

Consistent with the trends in 95th percentiles of daily IVT, the annual maximum daily rainfall indicates a decrease in summer and an increase in winter during the 1951–2020 period (Table 1 and Fig. 8a). Therefore, there is a shift in flood seasonality, with more floods occurring in the winter and fewer floods occurring in the summer during the second half of the 1957–2020 period (Figs. 8b,c). Apart from increased daily rainfall totals in winter, urbanization also plays a role in shifting flood seasonality because increased impervious cover can lead to substantial overland flows even with low-intensity winter storms (e.g., <1 mm h^{-1}) by increasing contributing area. Moreover, M–K tests for three SNOTEL sites show an increase in mean winter temperature and a decrease in winter peak SWE, although it is insignificant at the 5% level. This implies that winter precipitation, even in the high-elevation mountains, is increasingly likely to fall as rain in the future, exacerbating winter flood risk, especially for the city margins.

c. *Rainfall and flood hydrometeorology*

The hydrometeorology of flooding is examined through analyses of the spatial and temporal distributions of extreme rainfalls. We used NClimGrid data (5 km and daily) to analyze the spatial structure of daily rainfalls that caused the five largest winter and summer floods, respectively (Fig. 9). First, the spatial patterns of both winter and summer rainfalls in Fig. 9 show higher values around the mountains and lower values over the valley, highlighting the orographic effects on

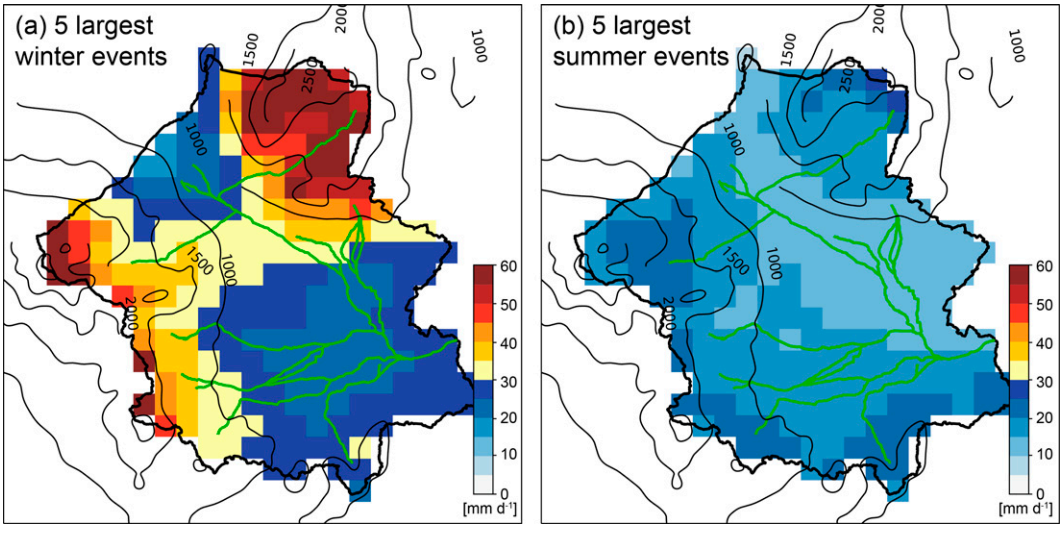

FIG. 9. The spatial distribution of composite daily rainfalls that caused the five largest (a) winter and (b) summer floods during the 1957–2020 period. The averaged rainfall for five winter and summer events are 34 and 17 mm day^{-1}, respectively. The averaged peak flows for five winter and summer events are 262 and 331 m^3 s^{-1}, respectively. Green line denotes the main river channels. Elevation contours are shown with 500-m intervals.

TABLE 2. Annual peak flows for the LVW watershed for the 1996–2020 period and the corresponding rainfall characteristics based on rain gauges. Peak flows are shown in descending order. The basin-averaged rainfall intensities represent the mean value using all available rain gauges.

Date	Peak flows ($m^3 s^{-1}$)	Duration (h)	Rainfall totals (mm)	Max 15-min rainfall intensities (mm h^{-1})	Max 1-h rainfall intensities (mm h^{-1})	Contribution of max 1-h rainfall (%)
8 Jul 1999	509	5.75	25	16	13	52
22 Aug 2012	470	8.75	25	7	6	25
12 Mar 2020	368	8.75	24	9	8	30
12 Oct 2012	308	19.75	25	5	4	15
29 Dec 2004	272	21.75	46	7	6	13
11 Sep 1998	272	8.5	12	5	4	36
22 Dec 2010	240	16	27	5	5	17
9 Apr 2016	229	9.75	7	2	2	24
21 Feb 2000	226	8.75	18	5	4	23
21 Jan 2010	205	11.5	18	3	3	17
9 Jan 2018	193	17.75	29	7	6	21
14 Feb 2019	151	12	29	4	4	12
18 Oct 2005	123	25	42	6	5	13
11 Aug 1997	109	4.25	5	3	3	51
7 Feb 2009	92	6.5	12	4	3	27
14 Sep 2006	86	15.25	15	5	4	26
19 Jul 2017	75	4	4	3	3	67
23 Feb 2015	74	9	11	3	2	23
28 Feb 2001	70	17.75	23	4	4	15
8 Sep 2014	69	7	10	5	4	38
7 Aug 2008	67	1.25	2	2	1	95
26 Feb 2003	57	15.75	20	2	2	12
23 Feb 2004	57	27.25	23	4	3	14
28 Jul 1996	13	2.5	3	4	2	73
24 Nov 2001	11	2.25	3	2	2	64

rainfall amounts. Second, the average rainfall depths of five summer storms are smaller than the value of five winter storms, but the summer storms yielded higher average flood peaks. This is consistent with Fig. 2b and the spatial patterns of rainfall that caused all summer and winter floods (Fig. S8), underscoring the high flood-generating efficiency of summer storms.

A dense network of rain gauges provides rainfall observations at higher spatial and temporal (i.e., 15 min) resolutions, facilitating spatiotemporal characterization of rainfall. The 25 storm events that caused the 1996–2020 annual flood peaks for the LVW watershed were analyzed with respect to their durations, rainfall totals, and maximum rainfall intensities (Table 2). Summer storms had relatively shorter durations but higher maximum 15-min and 1-h rainfall rates compared with winter storms (Table 2). For example, the September 1999 rainfall event, which caused the record flood, experienced rain rates at 8 gauges that exceeded 80 mm h^{-1} over a 15-min interval, which corresponds to the 100-yr recurrence interval based on NOAA Atlas 14 (Bonnin et al. 2011). In addition, rainfall totals during summer storms were largely (e.g., >50%) comprised of the most intense 1-h periods, whereas the corresponding portion of total rainfall during the most intense 1-h period for winter storms is smaller (e.g., <20%). The Pearson correlation coefficient between peak flows and rainfall totals is 0.38 (column 2 and 4 in Table 2) but reaches 0.70 between peak flows and maximum 1-h rainfall intensities (columns 2 and 6 in Table 2).

Rain-gauge-based rainfall totals for the largest four flood events also show distinct spatial patterns between summer and winter storms. The gradients of rainfall totals are from south to north for two summer storms (Figs. 10a,b), whereas they are from northwest to southeast for two winter storms (Figs. 10c,d). When heavy storm cells situate over the southern portions of the LVW watershed, flood flows experience shorter travel distances and less attenuation in channel and detention basins, leading to higher flood peaks. Conversely, the heavy rainfall of the two winter storms occurred over the northwestern portions of the watershed. This generated more attenuated flood waves. The distinct spatiotemporal structures for summer and winter storms driven by large-scale atmospheric circulations (i.e., hydroclimatology; section 4b) determine the variability in annual peak flows for both seasons regardless of urbanization.

The different storm characteristics in two seasons are closely linked to their corresponding synoptic-scale weather patterns. Winter storms are mainly driven by the continuous and strong moisture transport during a moist neutral atmosphere and thus storms are characterized by long duration (12–24 h) and low to moderate intensity (<5 mm h^{-1}) (Table 2; Fig. S7). In sharp contrast, summer storms occur when the heating of mountainous terrain triggers thunderstorm activity under moist and unstable atmospheric conditions that occur during NAM-related moisture surge. Summer storms produce rainfall with short durations (<6 h) and high intensities (>10 mm h^{-1}).

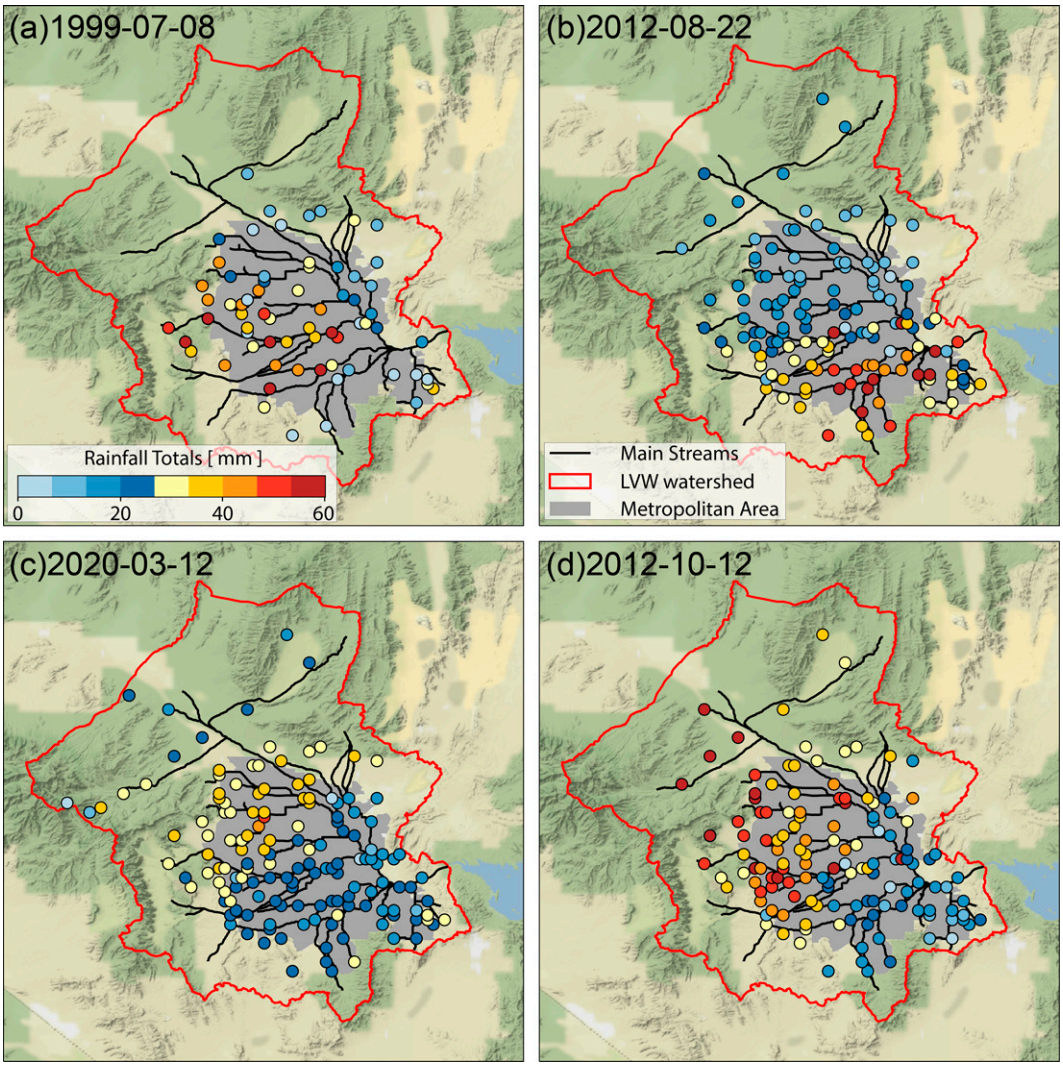

FIG. 10. The spatial distribution of rain gauge-based rainfall totals for the largest two (a),(b) summer and (c),(d) winter flood events.

5. Discussion

a. Stormwater management in arid regions

Stormwater management for urbanized watersheds in the arid and semiarid Southwestern United States primarily focuses on flood control (NRC 2009). Because cities are typically located on valley floors, the main objectives of flood control involve: 1) preventing runoff generated in upland areas from rapidly entering the urbanized area and 2) moving water away from the urbanized area to downstream as rapidly and safely as possible. For these reasons, flood conveyance systems in arid areas tend to be concrete lined. Although the constructed conveyance systems can impair water quality and ecological systems as well as reduce groundwater recharge, several examples (such as built channels in LVW and the Los Angeles River) have demonstrated their robust role in flood control (NRC 2009).

We found evidence that the increased flood peaks, especially after the mid-1990s, are very likely attributable to constructed flood conveyance rather than land-use change. This conclusion is primarily based on the co-occurrence between the detected changepoint in peak flows and the construction of flood conveyance systems. Without flood conveyance systems, overland flow must follow the land surface (e.g., roadways in urbanized areas) to reach natural channels, potentially causing the inundation of those surfaces and adjacent developed property in the process. On the contrary, a high density of flood conveyance systems can efficiently transport this flow to the watershed outlet, leading to higher flood peaks in compensation for less inundation. In other words, this reduces the urban flood risk in terms of the inundation depths and durations of developed land.

b. The importance of rainfall and flood mixtures

Peak flows and maximum daily rainfalls in the LVW watershed show two pronounced seasonality responses attributable to a mixture of two different hydrometeorological drivers

(i.e., flood-generating mechanisms). These phenomena are referred to as rainfall and flood mixtures (e.g., Yu et al. 2022), which have at least two important implications.

The first implication is related to climatic nonstationarity. The existence of rainfall and flood mixtures imply that efforts to identify trends are unlikely to succeed if they do not account for potential changes in the underlying "subsamples" associated with different physical drivers. Here, we show two distinct significant trends in annual maximum daily rainfall in summer and winter, which are consistent with changes in the 95th percentile daily IVT during these seasons (Fig. 8a; Table 1). Increases in winter rainfall and decreases in summer rainfall, interacting with land-use change have driven a shift in flood seasonality. A similar example can be found in Yu et al. (2019), which showed that the absence of a statistically significant trend in annual flood peaks in one midwestern watershed "missed" two significant trends: a decrease in spring snowmelt and rain-on-snow flooding, as well as an increase in summer flood peaks associated with mesoscale convective systems.

The second implication is related to frequency analyses of rainfall and floods, i.e., estimation of rainfall and flood quantiles, such as the so-called 100-yr events (e.g., Yu et al. 2022). Here, we show that winter and summer storms have different durations, spatiotemporal structures, and prevailing directions. Even assuming stationary climatic and non-climatic drivers, these distinct storm types generate flood peaks that should belong to two distinct populations. However, conventional flood frequency analysis approaches neglect different flood agents (i.e., the causes of the flood peaks), leading to potentially unrealistic estimates of flood quantiles, especially for the upper tail. For example, Klemeš (1986) argued that why should the probability of thunderstorms caused floods depend on snowmelt-driven floods. The issue of flood mixtures is prevalent across the western United States, with most watersheds experiencing two or more distinct flood drivers (e.g., atmospheric rivers, tropical cyclones, NAM, and snowmelt; Hirschboeck 1987a,b; Barth et al. 2017; Smith et al. 2018; Yu et al. 2022).

c. *Implications for urban flood forecasting*

This study provides a process-based understanding of the physical connection between large-scale drivers and local-scale flood responses that can facilitate operational flood forecasting. During the winter, El Niño and the associated increased frequency of low pressure systems and equatorward shift of the jet stream over the West Coast are typical precursors to strong ARs in the southern tier of North America. Forecasters should keep a watchful eye on the evolution of these ARs (e.g., landfall location orientation, intensity, duration, and other favorable mesoscale-synoptic patterns to induce heavy precipitation) because some of them may penetrate inland and affect precipitation patterns over southern Nevada (Neiman et al. 2013; Albano et al. 2020). During the monsoon season, forecasters should pay attention to the location and strength of the subtropical ridge that determines low- and midlevel moisture transported from the Gulf of California and the eastern Pacific to the southwestern United States (Adams and Comrie 1997; Higgins et al. 1997; Mitchell et al. 2002; Mazon et al. 2016).

6. Summary and conclusions

In this study, we examined nonstationary flood behavior for an urbanized watershed in the arid Southwestern United States from the perspectives of hydroclimatology, hydrometeorology, and hydrology. This study used USGS streamflow observations, gridded daily precipitation, 15-min rainfall observations from a network of 135 rain gauges, land-use reanalysis and observations, and atmospheric reanalysis. Based on these historical observations/reanalyses, the major findings are as follows:

1) The magnitude and variability in annual flood peaks for the LVW watershed have increased dramatically from 1957 to 2020, with a changepoint detected in 1996. Urbanization and the corresponding increase in imperviousness within the valley are roughly linear with time, in contrast to a supra-linear increase in flood peaks since the mid-1990s. This "accelerating" increase in flood peaks since that time is very likely attributable to the implementation of widespread flood conveyance facilities since the 1990s. Elaboration of drainage networks and channel lining increase hydrologic connectivity and reduce hydrologic response time, which enhance flood peaks. The detention basins play a role in attenuating flood peaks at the event scale, but their overall performance in mitigating the impacts of urbanization at the watershed scale is less effective.
2) Extreme rainfall and floods for the LVW watershed show pronounced seasonality associated with large-scale hydrometeorological drivers. The jet stream drives the moisture from the eastern Pacific eastward in winter whereas circulations associated with the NAM drive the moisture from the Gulfs of California and Mexico northward in summer. Winter storms for the LVW watershed are also associated with inland-penetrating ARs, which are teleconnected with ENSO. Summer rainfalls are tied to thunderstorms, with the NAM fueling the moisture and instability from the south and local surface heating helping trigger instability. These findings demonstrate that local-scale events are often embedded within larger-scale weather systems.
3) Hydrometeorological drivers for winter and summer floods both show statistically significant changes over time, albeit in different directions. The 95th percentile of daily water vapor transport (IVT) and maximum daily summer rainfall show decreasing trends whereas their winter counterparts show increasing trends. Urbanization in the watershed also plays a role in enhancing winter floods because less intense winter rain falling on impervious surfaces can still yield substantial runoff. Therefore, flood seasonality for the LVW watershed has shifted from the summer to the winter, even as floods have grown more variable and extreme. This highlights that deeper examination of the meteorological causes of extreme rainfall and floods can

lead to a better understanding of their trends and if they will continue under projected warming.

4) Given similar daily rainfalls, summer storms tend to yield higher flood peaks than winter storms, irrespective of urbanization. This is because of the difference in the spatiotemporal distributions of storms. Using a dense network of rain gauges, we show that summer storms have high intensity over small areas and short durations, whereas winter storms have larger spatial extents and longer durations, but are less intense in terms of peak rain rates.
5) The complex flood hydrology of the LVW watershed is a clear example that "stationarity is dead" (Milly et al. 2008). Its nonstationarities arises from a combination of land-use change, implementation of conveyance facilities (i.e., step change), low-frequency internal climate variability (i.e., ENSO), and a shift in flood seasonality stemming from distinct trends in summer and winter storms.

This analysis presents previously under-documented features of large-scale hydroclimatology, regional-scale hydrometeorology, and local-scale hydrology, and their joint effects on urban flooding in the arid region. By integrating data from long-term observations and reanalysis, we provide insights into nonstationarities in individual flood agents and their interactions in driving changes in flood magnitudes and seasonality. This study demonstrates that complex processes involving climatic and non-climatic drivers results in nonstationarity in flood observations. Therefore, process-based approaches are critical to understanding and examining nonstationary flood hydrology. Finally, we highlighted the potentials in transferring the knowledge developed from this study to operational hydrology, including flood frequency analysis (e.g., England et al. 2014; Wright et al. 2014; Yu et al. 2019, 2020, 2021) and flood forecasting (e.g., Doswell et al. 1996; Davis 2001; Doswell and Schultz 2006).

Acknowledgments. GY's contribution was supported by the Desert Research Institute Maki Postdoctoral Fellowship. JM's, BH's, and MB's contributions were supported by the Desert Research Institute. DBW's contribution was supported by the University of Wisconsin– Madison. ZZ's contribution was supported by the National Natural Science Foundation of China (52009021). We thank Nicole Damon at Desert Research Institute for her assistance on technical editing. Additionally, we thank editor Dr. L. Ruby Leung, along with two anonymous reviewers, for their insightful suggestions that helped improve the overall quality of this manuscript.

Data availability statement. USGS-LU and NLCD land-use data are available at https://doi.org/10.5066/F7KK99RR and https://www.mrlc.gov/, respectively. NClimGrid daily precipitation data are available from NOAA/NCEI at https://www.ncei.noaa.gov/access/metadata/landing-page/bin/iso?id=gov.noaa.ncdc:C00332. ERA5 reanalysis is available from the Climate Data Store at https://cds.climate.copernicus.eu/. Annual peak flow data for all the stream gages within the Las Vegas Wash watershed is available from USGS at https://waterdata.usgs.gov/nwis. NHDPlus V2 is available from USGS at https://nhdplus.com/NHDPlus/NHDPlusV2_home.php. Rain gauge and flood conveyance data are available from the Clark County Regional Flood Control District at https://www.regionalflood.org/programs-services/rainfall-and-weather/historical-rainfall/gage-data.

REFERENCES

Adams, D. K., and A. C. Comrie, 1997: The North American monsoon. *Bull. Amer. Meteor. Soc.*, **78**, 2197–2214, https://doi.org/10.1175/1520-0477(1997)078<2197:TNAM>2.0.CO;2.

Ahmadalipour, A., and H. Moradkhani, 2019: A data-driven analysis of flash flood hazard, fatalities, and damages over the CONUS during 1996–2017. *J. Hydrol.*, **578**, 124106, https://doi.org/10.1016/j.jhydrol.2019.124106.

Albano, C. M., M. D. Dettinger, and A. A. Harpold, 2020: Patterns and drivers of atmospheric river precipitation and hydrologic impacts across the western United States. *J. Hydrometeor.*, **21**, 143–159, https://doi.org/10.1175/JHM-D-19-0119.1.

Augustine, J. A., J. J. DeLuisi, and C. N. Long, 2000: SURFRAD–A national surface radiation budget network for atmospheric research. *Bull. Amer. Meteor. Soc.*, **81**, 2341–2358, https://doi.org/10.1175/1520-0477(2000)081<2341:SANSRB>2.3.CO;2.

Baek, S. H., and J. M. Lora, 2021: Counterbalancing influences of aerosols and greenhouse gases on atmospheric rivers. *Nat. Climate Change*, **11**, 958–965, https://doi.org/10.1038/s41558-021-01166-8.

Barnett, T. P., and Coauthors, 2008: Human-induced changes in the hydrology of the western United States. *Science*, **319**, 1080–1083, https://doi.org/10.1126/science.1152538.

Barth, N. A., G. Villarini, M. A. Nayak, and K. White, 2017: Mixed populations and annual flood frequency estimates in the western United States: The role of atmospheric rivers. *Water Resour. Res.*, **53**, 257–269, https://doi.org/10.1002/2016WR019064.

——, ——, and K. White, 2018: Contribution of eastern North Pacific tropical cyclones and their remnants on flooding in the western United States. *Int. J. Climatol.*, **38**, 5441–5446, https://doi.org/10.1002/joc.5735.

Beighley, R. E., and G. E. Moglen, 2002: Trend assessment in rainfall-runoff behavior in urbanizing watersheds. *J. Hydrol. Eng.*, **7**, 27–34, https://doi.org/10.1061/(ASCE)1084-0699(2002)7:1(27).

——, and ——, 2003: Adjusting measured peak discharges from an urbanizing watershed to reflect a stationary land use signal. *Water Resour. Res.*, **39**, 1093, https://doi.org/10.1029/2002WR001846.

Berg, W. K., D. M. Anderson, and J. J. Bates, 2000: Satellite observations of a Pacific moisture surge associated with flooding in Las Vegas. *Geophys. Res. Lett.*, **27**, 2553–2556, https://doi.org/10.1029/2000GL011367.

Bonnin, G. M., D. Martin, B. Lin, T. Parzybok, M. Yekta, and D. Riley, 2011: Precipitation-frequency atlas of the United States, version 5.0. Vol. 1, NOAA Atlas 14, 265 pp., https://www.weather.gov/media/owp/oh/hdsc/docs/Atlas14_Volume1.pdf.

Burns, D., T. Vitvar, J. McDonnell, J. Hassett, J. Duncan, and C. Kendall, 2005: Effects of suburban development on runoff

generation in the Croton River basin, New York, USA. *J. Hydrol.*, **311**, 266–281, https://doi.org/10.1016/j.jhydrol.2005.01.022.

Cayan, D. R., K. T. Redmond, and L. G. Riddle, 1999: ENSO and hydrologic extremes in the western United States. *J. Climate*, **12**, 2881–2893, https://doi.org/10.1175/1520-0442(1999)012<2881:EAHEIT>2.0.CO;2.

Choi, J.-Y., B. A. Engel, S. Muthukrishnan, and J. Harbor, 2003: GIS based long term hydrologic impact evaluation for watershed urbanization. *J. Amer. Water Resour. Assoc.*, **39**, 623–635, https://doi.org/10.1111/j.1752-1688.2003.tb03680.x.

Cleveland, W. S., 1979: Robust locally weighted regression and smoothing scatterplots. *J. Amer. Stat. Assoc.*, **74**, 829–836, https://doi.org/10.1080/01621459.1979.10481038.

Coe, J. A., 2016: Landslide hazards and climate change: A perspective from the United States. *Slope Safety Preparedness for Impact of Climate Change*, K. Ho, S. Lacasse, and L. Picarelli, Eds., 1st ed. CRC Press, 479–524.

Costa, J. E., 1987: Hydraulics and basin morphometry of the largest flash floods in the conterminous United States. *J. Hydrol.*, **93**, 313–338, https://doi.org/10.1016/0022-1694(87)90102-8.

Culley, S., S. Noble, A. Yates, M. Timbs, S. Westra, H. R. Maier, M. Giuliani, and A. Castelletti, 2016: A bottom-up approach to identifying the maximum operational adaptive capacity of water resource systems to a changing climate. *Water Resour. Res.*, **52**, 6751–6768, https://doi.org/10.1002/2015WR018253.

Davis, R. S., 2001: Flash flood forecast and detection methods. *Severe Convective Storms*, *Meteor. Monogr.*, No. 50, Amer. Meteor. Soc., 481–525.

Doswell, C. A., III, and D. M. Schultz, 2006: On the use of indices and parameters in forecasting severe storms. *Electron. J. Severe Storms Meteor.*, **1** (3), https://doi.org/10.55599/ejssm.v1i3.4.

——, H. E. Brooks, and R. A. Maddox, 1996: Flash flood forecasting: An ingredients-based methodology. *Wea. Forecasting*, **11**, 560–581, https://doi.org/10.1175/1520-0434(1996)011<0560:FFFAIB>2.0.CO;2.

England, J. F., P. Y. Julien, and M. L. Velleux, 2014: Physically-based extreme flood frequency with stochastic storm transposition and paleo flood data on large watersheds. *J. Hydrol.*, **510**, 228–245, https://doi.org/10.1016/j.jhydrol.2013.12.021.

Etheredge, D., D. S. Gutzler, and F. J. Pazzaglia, 2004: Geomorphic response to seasonal variations in rainfall in the Southwest United States. *Geol. Soc. Amer. Bull.*, **116**, 606–618, https://doi.org/10.1130/B22103.1.

Fowler, H. J., and Coauthors, 2021: Anthropogenic intensification of short-duration rainfall extremes. *Nat. Rev. Earth Environ.*, **2**, 107–122, https://doi.org/10.1038/s43017-020-00128-6.

Fry, J. A., and Coauthors, 2011: Completion of the 2006 national land cover database for the conterminous United States. *Photogramm. Eng. Remote Sens.*, **77**, 858–864.

Gershunov, A., T. Shulgina, F. M. Ralph, D. A. Lavers, and J. J. Rutz, 2017: Assessing the climate-scale variability of atmospheric rivers affecting western North America. *Geophys. Res. Lett.*, **44**, 7900–7908, https://doi.org/10.1002/2017GL074175.

——, and Coauthors, 2019: Precipitation regime change in western North America: The role of atmospheric rivers. *Sci. Rep.*, **9**, 9944, https://doi.org/10.1038/s41598-019-46169-w.

Glancy, P. A., and L. Harmsen, 1975: A hydrologic assessment of the September 14, 1974, flood in Eldorado Canyon, Nevada. Professional Paper 930, 28 pp., https://doi.org/10.3133/pp930.

Gupta, V. K., and O. J. Mesa, 1988: Runoff generation and hydrologic response via channel network geomorphology—Recent progress and open problems. *J. Hydrol.*, **102**, 3–28, https://doi.org/10.1016/0022-1694(88)90089-3.

——, E. Waymire, and C. T. Wang, 1980: A representation of an instantaneous unit hydrograph from geomorphology. *Water Resour. Res.*, **16**, 855–862, https://doi.org/10.1029/WR016i005p00855.

Hatchett, B. J., S. Burak, J. J. Rutz, N. S. Oakley, E. H. Bair, and M. L. Kaplan, 2017: Avalanche fatalities during atmospheric river events in the western United States. *J. Hydrometeor.*, **18**, 1359–1374, https://doi.org/10.1175/JHM-D-16-0219.1.

Hernandez, M., and L. Chen, 2022: Future land precipitation changes over the North American monsoon region using CMIP5 and CMIP6 Simulations. *J. Geophys. Res. Atmos.*, **127**, e2021JD035911, https://doi.org/10.1029/2021JD035911.

Hersbach, H., and Coauthors, 2020: The ERA5 global reanalysis. *Quart. J. Roy. Meteor. Soc.*, **146**, 1999–2049, https://doi.org/10.1002/qj.3803.

Higgins, R. W., Y. Yao, and X. L. Wang, 1997: Influence of the North American monsoon system on the U.S. summer precipitation regime. *J. Climate*, **10**, 2600–2622, https://doi.org/10.1175/1520-0442(1997)010<2600:IOTNAM>2.0.CO;2.

——, K. C. Mo, and Y. Yao, 1998: Interannual variability of the U.S. summer precipitation regime with emphasis on the southwestern monsoon. *J. Climate*, **11**, 2582–2606, https://doi.org/10.1175/1520-0442(1998)011<2582:IVOTUS>2.0.CO;2.

——, Y. Chen, and A. V. Douglas, 1999: Interannual variability of the North American warm season precipitation regime. *J. Climate*, **12**, 653–680, https://doi.org/10.1175/1520-0442(1999)012<0653:IVOTNA>2.0.CO;2.

Hirschboeck, K. K., 1987a: Catastrophic flooding and atmospheric circulation anomalies. *Catastrophic Flooding*, 1st ed. L. Mayer and D. B. Nash, Eds., Routledge, 23–56.

——, 1987b: Hydroclimatically-defined mixed distributions in partial duration flood series. *Hydrologic Frequency Modeling*, V. P. Singh, Ed., Springer, 199–212.

Hodgkins, G. A., R. W. Dudley, S. A. Archfield, and B. Renard, 2019: Effects of climate, regulation, and urbanization on historical flood trends in the United States. *J. Hydrol.*, **573**, 697–709, https://doi.org/10.1016/j.jhydrol.2019.03.102.

Homer, C., and Coauthors, 2020: Conterminous United States land cover change patterns 2001–2016 from the 2016 national land cover database. *ISPRS J. Photogramm. Remote Sens.*, **162**, 184–199, https://doi.org/10.1016/j.isprsjprs.2020.02.019.

Jiang, T., Y. D. Chen, C. Xu, X. Chen, X. Chen, and V. P. Singh, 2007: Comparison of hydrological impacts of climate change simulated by six hydrological models in the Dongjiang Basin, South China. *J. Hydrol.*, **336**, 316–333, https://doi.org/10.1016/j.jhydrol.2007.01.010.

Karl, T. R., J. M. Melillo, T. C. Peterson, and S. J. Hassol, 2009: *Global Climate Change Impacts in the United States*. Cambridge University Press, 188 pp.

Kendall, M. G., 1975: *Rank Correlation Methods*. 4th ed. 2nd impression, Charles Griffin and Company Ltd., 202 pp.

Kennedy, J. R., D. C. Goodrich, and C. L. Unkrich, 2013: Using the KINEROS2 modeling framework to evaluate the increase in storm runoff from residential development in a semiarid environment. *J. Hydrol. Eng.*, **18**, 698–706, https://doi.org/10.1061/(ASCE)HE.1943-5584.0000655.

Kilsby, C. G., S. S. Tellier, H. J. Fowler, and T. R. Howels, 2007: Hydrological impacts of climate change on the Tejo and Guadiana Rivers. *Hydrol. Earth Syst. Sci.*, **11**, 1175–1189, https://doi.org/10.5194/hess-11-1175-2007.

Kirshen, D. M., and R. L. Bras, 1983: The linear channel and its effect on the geomorphologic IUH. *J. Hydrol.*, **65**, 175–208, https://doi.org/10.1016/0022-1694(83)90216-0.

Klemeš, V., 1986: Dilettantism in hydrology: Transition or destiny? *Water Resour. Res.*, **22**, 177S–188S, https://doi.org/10.1029/WR022i09Sp0177S.

Koehler, T. L., 2020: Cloud-to-ground lightning flash density and thunderstorm day distributions over the contiguous United States derived from NLDN measurements: 1993–2018. *Mon. Wea. Rev.*, **148**, 313–332, https://doi.org/10.1175/MWR-D-19-0211.1.

Korhonen, J., and E. Kuusisto, 2010: Long-term changes in the discharge regime in Finland. *Hydrol. Res.*, **41**, 253–268, https://doi.org/10.2166/nh.2010.112.

Lee, M. T., and J. W. Delleur, 1976: A variable source area model of the rainfall-runoff process based on the watershed stream network. *Water Resour. Res.*, **12**, 1029–1036, https://doi.org/10.1029/WR012i005p01029.

Leopold, L. B., 1968: Hydrology for urban land planning—A guidebook on the hydrologic effects of urban land use. Geolgoical Survey Circular 554, 26 pp., https://pubs.usgs.gov/circ/1968/0554/report.pdf.

——, and T. Maddock Jr., 1953: The hydraulic geometry of stream channels and some physiographic implications. USGS Professional Paper 252, 57 pp., http://pubs.usgs.gov/pp/0252/report.pdf.

Li, J., R. A. Maddox, X. Gao, S. Sorooshian, and K. Hsu, 2003: A numerical investigation of storm structure and evolution during the July 1999 Las Vegas flash flood. *Mon. Wea. Rev.*, **131**, 2038–2059, https://doi.org/10.1175/1520-0493(2003)131<2038:ANIOSS>2.0.CO;2.

Maddox, R. A., F. Canova, and L. R. Hoxit, 1980: Meteorological characteristics of flash flood events over the western United States. *Mon. Wea. Rev.*, **108**, 1866–1877, https://doi.org/10.1175/1520-0493(1980)108<1866:MCOFFE>2.0.CO;2.

Mallakpour, I., and G. Villarini, 2017: Analysis of changes in the magnitude, frequency, and seasonality of heavy precipitation over the contiguous USA. *Theor. Appl. Climatol.*, **130**, 345–363, https://doi.org/10.1007/s00704-016-1881-z.

Mann, H. B., 1945: Nonparametric tests against trend. *Econometrica*, **13**, 245–259, https://doi.org/10.2307/1907187.

Mazon, J. J., C. L. Castro, D. K. Adams, H.-I. Chang, C. M. Carrillo, and J. J. Brost, 2016: Objective climatological analysis of extreme weather events in Arizona during the North American monsoon. *J. Appl. Meteor. Climatol.*, **55**, 2431–2450, https://doi.org/10.1175/JAMC-D-16-0075.1.

McCuen, R. H., 2002: *Modeling Hydrologic Change: Statistical Methods*. CRC Press, 448 pp.

Merz, R., and G. Blöschl, 2008: Flood frequency hydrology: 1. Temporal, spatial, and causal expansion of information. *Water Resour. Res.*, **44**, W08432, https://doi.org/10.1029/2007WR006744.

Michaelis, A. C., A. Gershunov, A. Weyant, M. A. Fish, T. Shulgina, and F. M. Ralph, 2022: Atmospheric river precipitation enhanced by climate change: A case study of the storm that contributed to California's Oroville Dam crisis. *Earth's Future*, **10**, e2021EF002537, https://doi.org/10.1029/2021EF002537.

Miller, J. J., 2012: Geologic and hydraulic concepts of arid environments. *Flood Hazard Identification and Mitigation in Semi-And Arid Environments*, R. H. French and J. J. Miller, Eds., World Scientific, 19–35.

——, S. A. Mizell, R. H. French, D. G. Meadows, and M. H. Young, 2012: Results of channel transmission loss studies during ephemeral flow events. *World Environmental and Water Resources Congress 2007*, Reston, VA, ASCE, 1–10, https://doi.org/10.1061/40927(243)610.

Milly, P. C. D., J. Betancourt, M. Falkenmark, R. M. Hirsch, Z. W. Kundzewicz, D. P. Lettenmaier, and R. J. Stouffer, 2008: Stationarity is dead: Whither water management? *Science*, **319**, 573–574, https://doi.org/10.1126/science.1151915.

Mitchell, D. L., D. Ivanova, R. Rabin, T. J. Brown, and K. Redmond, 2002: Gulf of California Sea surface temperatures and the North American monsoon: Mechanistic implications from observations. *J. Climate*, **15**, 2261–2281, https://doi.org/10.1175/1520-0442(2002)015<2261:GOCSST>2.0.CO;2.

Moore, R. B., and T. G. Dewald, 2016: The road to NHDPlus—Advancements in digital stream networks and associated catchments. *J. Amer. Water Resour. Assoc.*, **52**, 890–900, https://doi.org/10.1111/1752-1688.12389.

Neiman, P. J., F. M. Ralph, B. J. Moore, M. Hughes, K. M. Mahoney, J. M. Cordeira, and M. D. Dettinger, 2013: The landfall and inland penetration of a flood-producing atmospheric river in Arizona. Part I: Observed synoptic-scale, orographic, and hydrometeorological characteristics. *J. Hydrometeor.*, **14**, 460–484, https://doi.org/10.1175/JHM-D-12-0101.1.

NOAA, 2022: Southern oscillation index (SOI)—El Niño/Southern Oscillation (ENSO). National Centers for Environmental Information (NCEI), accessed 6 September 2022, https://www.ncei.noaa.gov/access/monitoring/enso/soi.

NRC, 2009: *Urban Stormwater Management in the United States*. National Academies Press, 587 pp.

Oudin, L., B. Salavati, C. Furusho-Percot, P. Ribstein, and M. Saadi, 2018: Hydrological impacts of urbanization at the catchment scale. *J. Hydrol.*, **559**, 774–786, https://doi.org/10.1016/j.jhydrol.2018.02.064.

Pascale, S., W. R. Boos, S. Bordoni, T. L. Delworth, S. B. Kapnick, H. Murakami, G. A. Vecchi, and W. Zhang, 2017: Weakening of the North American monsoon with global warming. *Nat. Climate Change*, **7**, 806–812, https://doi.org/10.1038/nclimate3412.

Perez, G., R. Mantilla, and W. F. Krajewski, 2018: The influence of spatial variability of width functions on regional peak flow regressions. *Water Resour. Res.*, **54**, 7651–7669, https://doi.org/10.1029/2018WR023509.

Petrow, T., and B. Merz, 2009: Trends in flood magnitude, frequency and seasonality in Germany in the period 1951–2002. *J. Hydrol.*, **371**, 129–141, https://doi.org/10.1016/j.jhydrol.2009.03.024.

Pettitt, A. N., 1979: A non-parametric approach to the change-point problem. *J. Roy. Stat. Soc.*, **28C**, 126–135, https://doi.org/10.2307/2346729.

Pierce, D. W., and Coauthors, 2008: Attribution of declining western U.S. snowpack to human effects. *J. Climate*, **21**, 6425–6444, https://doi.org/10.1175/2008JCLI2405.1.

Polade, S. D., A. Gershunov, D. R. Cayan, M. D. Dettinger, and D. W. Pierce, 2017: Precipitation in a warming world: Assessing projected hydro-climate changes in California and other Mediterranean climate regions. *Sci. Rep.*, **7**, 10783, https://doi.org/10.1038/s41598-017-11285-y.

Prein, A. F., R. M. Rasmussen, K. Ikeda, C. Liu, M. P. Clark, and G. J. Holland, 2017: The future intensification of hourly precipitation extremes. *Nat. Climate Change*, **7**, 48–52, https://doi.org/10.1038/nclimate3168.

Ralph, F. M., J. J. Rutz, J. M. Cordeira, M. Dettinger, M. Anderson, D. Reynolds, L. J. Schick, and C. Smallcomb, 2019: A scale to characterize the strength and impacts of atmospheric rivers. *Bull. Amer. Meteor. Soc.*, **100**, 269–289, https://doi.org/10.1175/BAMS-D-18-0023.1.

Randerson, D., 1976: Meteorological analysis for the Las Vegas, Nevada, Flood of 3 July 1975. *Mon. Wea. Rev.*, **104**, 719–727, https://doi.org/10.1175/1520-0493(1976)104<0719:MAFTLV>2.0.CO;2.

Redmond, K. T., and R. W. Koch, 1991: Surface climate and streamflow variability in the western United States and their relationship to large-scale circulation indices. *Water Resour. Res.*, **27**, 2381–2399, https://doi.org/10.1029/91WR00690.

Rhoades, A. M., and Coauthors, 2020: The shifting scales of western U.S. landfalling atmospheric rivers under climate change. *Geophys. Res. Lett.*, **47**, e2020GL089096, https://doi.org/10.1029/2020GL089096.

Rodríguez-Iturbe, I., and A. Rinaldo, 2001: *Fractal River Basins: Chance and Self-Organization*. Cambridge University Press, 574 pp.

Rutz, J. J., W. J. Steenburgh, and F. M. Ralph, 2014: Climatological characteristics of atmospheric rivers and their inland penetration over the western United States. *Mon. Wea. Rev.*, **142**, 905–921, https://doi.org/10.1175/MWR-D-13-00168.1.

——, ——, and ——, 2015: The inland penetration of atmospheric rivers over western North America: A Lagrangian analysis. *Mon. Wea. Rev.*, **143**, 1924–1944, https://doi.org/10.1175/MWR-D-14-00288.1.

Sauer, V. B., W. O. Thomas Jr., V. A. Stricker, and K. V. Wilson, 1983: Flood characteristics of urban watersheds in the United States. U.S. Geological Survey, Water Supply Paper 2207, 69 pp., https://doi.org/10.3133/wsp2207.

Sen, P. K., 1968: Estimates of the regression coefficient based on Kendall's tau. *J. Amer. Stat. Assoc.*, **63**, 1379–1389, https://doi.org/10.1080/01621459.1968.10480934.

Sheppard, P. R., A. C. Comrie, G. D. Packin, K. Angersbach, and M. K. Hughes, 2002: The climate of the U.S. Southwest. *Climate Res.*, **21**, 219–238, https://doi.org/10.3354/cr021219.

Siirila-Woodburn, E. R., and Coauthors, 2021: A low-to-no snow future and its impacts on water resources in the western United States. *Nat. Rev. Earth Environ.*, **2**, 800–819, https://doi.org/10.1038/s43017-021-00219-y.

Singer, M. B., and K. Michaelides, 2017: Deciphering the expression of climate change within the lower Colorado River basin by stochastic simulation of convective rainfall. *Environ. Res. Lett.*, **12**, 104011, https://doi.org/10.1088/1748-9326/aa8e50.

Smith, J. A., M. L. Baeck, J. E. Morrison, P. Sturdevant-Rees, D. F. Turner-Gillespie, and P. D. Bates, 2002: The regional hydrology of extreme floods in an urbanizing drainage basin. *J. Hydrometeor.*, **3**, 267–282, https://doi.org/10.1175/1525-7541(2002)003<0267:TRHOEF>2.0.CO;2.

——, ——, K. L. Meierdiercks, P. A. Nelson, A. J. Miller, and E. J. Holland, 2005a: Field studies of the storm event hydrologic response in an urbanizing watershed. *Water Resour. Res.*, **41**, W10413, https://doi.org/10.1029/2004WR003712.

——, A. J. Miller, M. L. Baeck, P. A. Nelson, G. T. Fisher, and K. L. Meierdiercks, 2005b: Extraordinary flood response of a small urban watershed to short-duration convective rainfall. *J. Hydrometeor.*, **6**, 599–617, https://doi.org/10.1175/JHM426.1.

——, A. A. Cox, M. L. Baeck, L. Yang, and P. Bates, 2018: Strange floods: The upper tail of flood peaks in the United States. *Water Resour. Res.*, **54**, 6510–6542, https://doi.org/10.1029/2018WR022539.

——, M. L. Baeck, L. Yang, J. Signell, E. Morin, and D. C. Goodrich, 2019: The paroxysmal precipitation of the desert: Flash floods in the southwestern United States. *Water Resour. Res.*, **55**, 10 218–10 247, https://doi.org/10.1029/2019WR025480.

Smith, W., 1986: The effects of Eastern North Pacific tropical cyclones on the Southwestern United States. NOAA Tech. Memo. NWS WR 197, 264 pp., https://repository.library.noaa.gov/view/noaa/7105.

Sohl, T., R. R. Reker, M. A. Bouchard, K. L. Sayler, J. Dornbierer, S. Wika, R. Quenzer, and A. M. Friesz, 2016: Modeled historical land use and land cover for the conterminous United States. *J. Land Use Sci.*, **11**, 476–499, https://doi.org/10.1080/1747423X.2016.1147619.

Swales, D., M. Alexander, and M. Hughes, 2016: Examining moisture pathways and extreme precipitation in the U.S. Intermountain West using self-organizing maps. *Geophys. Res. Lett.*, **43**, 1727–1735, https://doi.org/10.1002/2015GL067478.

Tarboton, D. G., R. L. Bras, and I. Rodriguez-Iturbe, 1989: Scaling and elevation in river networks. *Water Resour. Res.*, **25**, 2037–2051, https://doi.org/10.1029/WR025i009p02037.

Thomas, B. E., H. W. Hjalmarson, and S. D. Waltemeyer, 1997: Methods for estimating magnitude and frequency of floods in the southwestern United States. USGS Water Supply Paper 2433, 195 pp., https://doi.org/10.3133/wsp2433.

U.S. Census Bureau, 2020: Census of population and housing. U.S. Census Bureau, accessed 6 September 2022, https://www.census.gov/library/visualizations/interactive/2020-population-and-housing-state-data.html.

Veitzer, S. A., and V. K. Gupta, 2001: Statistical self-similarity of width function maxima with implications to floods. *Adv. Water Resour.*, **24**, 955–965, https://doi.org/10.1016/S0309-1708(01)00030-6.

Vose, R., and Coauthors, 2014: Gridded 5 km GHCN-daily temperature and precipitation dataset (nCLIMGRID) version 1. NOAA/National Centers for Environmental Information, accessed 6 December 2014, https://doi.org/10.7289/V5SX6B56.

Wright, D. B., J. A. Smith, G. Villarini, and M. L. Baeck, 2012: Hydroclimatology of flash flooding in Atlanta. *Water Resour. Res.*, **48**, W04524, https://doi.org/10.1029/2011WR011371.

——, ——, and M. L. Baeck, 2014: Flood frequency analysis using radar rainfall fields and stochastic storm transposition. *Water Resour. Res.*, **50**, 1592–1615, https://doi.org/10.1002/2013WR014224.

——, G. Yu, and J. F. England, 2020: Six decades of rainfall and flood frequency analysis using stochastic storm transposition: Review, progress, and prospects. *J. Hydrol.*, **585**, 124816, https://doi.org/10.1016/j.jhydrol.2020.124816.

Wright, W. E., A. Long, A. C. Comrie, S. W. Leavitt, T. Cavazos, and C. Eastoe, 2001: Monsoonal moisture sources revealed using temperature, precipitation, and precipitation stable isotope time series. *Geophys. Res. Lett.*, **28**, 787–790, https://doi.org/10.1029/2000GL012094.

Yang, L., J. A. Smith, D. B. Wright, M. L. Baeck, G. Villarini, F. Tian, and H. Hu, 2013: Urbanization and climate change: An examination of nonstationarities in urban flooding. *J. Hydrometeor.*, **14**, 1791–1809, https://doi.org/10.1175/JHM-D-12-095.1.

Yu, G., D. B. Wright, Z. Zhu, C. Smith, and K. D. Holman, 2019: Process-based flood frequency analysis in an agricultural

watershed exhibiting nonstationary flood seasonality. *Hydrol. Earth Syst. Sci.*, **23**, 2225–2243, https://doi.org/10.5194/hess-23-2225-2019.

——, ——, and Z. Li, 2020: The upper tail of precipitation in convection-permitting regional climate models and their utility in nonstationary rainfall and flood frequency analysis. *Earth's Future*, **8**, e2020EF001613, https://doi.org/10.1029/2020EF001613.

——, ——, and K. D. Holman, 2021: Connecting hydrometeorological processes to low-probability floods in the mountainous Colorado front range. *Water Resour. Res.*, **57**, e2021WR029768, https://doi.org/10.1029/2021WR029768.

——, ——, and F. V. Davenport, 2022: Diverse physical processes drive upper-tail flood quantiles in the U.S. mountain west. *Geophys. Res. Lett.*, **49**, e2022GL098855, https://doi.org/10.1029/2022GL098855.